



# Delivery of deep-sourced, volatile-rich plume material to the global ridge system

Sally A. Gibson<sup>a,\*</sup>, Mark A. Richards<sup>b,1</sup>

<sup>a</sup> Department of Earth Sciences, University of Cambridge, Cambridge, UK

<sup>b</sup> Department of Earth and Planetary Science, University of California, Berkeley, CA, USA

## ARTICLE INFO

### Article history:

Received 1 March 2018

Received in revised form 17 July 2018

Accepted 19 July 2018

Available online 3 August 2018

Editor: T.A. Mather

### Keywords:

volatiles

mantle plumes

OIB

MORB

plume–ridge interaction

## ABSTRACT

The global mid-ocean ridge (MOR) system represents a major site for outgassing of volatiles from Earth's mantle. The amount of H<sub>2</sub>O released via eruption of mid-ocean ridge basalts varies along the global ridge system and greatest at sites of interaction with mantle plumes. These deep-sourced thermal anomalies affect approximately one-third of all MORs – as reflected in enrichment of incompatible trace elements, isotope signatures and elevated ridge topography (excess melting) – but the physical mechanisms involved are controversial. The “standard model” involves solid-state flow interaction, wherein an actively upwelling plume influences the divergent upwelling generated by a mid-ocean ridge so that melting occurs at higher pressures and in greater amounts than at a normal spreading ridge. This model does not explain, however, certain enigmatic features including linear volcanic ridges radiating from the active plume to the nearby MOR. Examples of these are the Wolf–Darwin lineament (Galápagos), Rodrigues Ridge (La Réunion), Discovery Ridge (Discovery), and numerous smaller ridge-like structures associated with the Azores and Easter–Salas y Gómez hot spots. An important observation from our study is that fractionation-corrected MORB with exceptionally-high H<sub>2</sub>O contents (up to 1.3 wt.%) are found in close proximity to intersections of long-lived plume-related volcanic lineaments with spreading centres. New algorithms in the rare-earth element inversion melting (INVMEL) program allow us to simulate plume–ridge interactions by mixing the compositions of volatile-bearing melts generated during both active upwelling and passively-driven corner-flow. Our findings from these empirical models suggest that at sites of plume–ridge interaction, moderately-enriched MORBs (with 0.2–0.4 wt.% H<sub>2</sub>O) result from mixing of melts formed by: (i) active upwelling of plume material to minimum depths of ~35 km; and (ii) those generated by passive melting at shallower depths beneath the ridge. The most volatile-rich MORB (0.4–1.3 wt.% H<sub>2</sub>O) may form by the further addition of up to 25% of “deep” small-fraction plume stem melts that contain >3 wt.% H<sub>2</sub>O. We propose that these volatile-rich melts are transported directly to nearby MOR segments via pressure-induced, highly-channelised flow embedded within a broader “puddle” of mostly solid-state plume material, spreading beneath the plate as a gravity flow. This accounts for the short wavelength variability (over 10s of km) in geochemistry and bathymetry that is superimposed on the much larger (many 100s of km) “waist width” of plume-influenced ridge. Melt channels may constitute a primary delivery mechanism for volatiles from plume stems to nearby MORs and, in some instances, be expressed at the surface as volcanic lineaments and ridges. The delivery of small-fraction hydrous melts from plume stems to ridges via a two-phase (melt–matrix) regime implies that a parallel, bimodal transport system is involved at sites of plume–ridge interaction. We estimate that the rate of emplacement of deep-sourced volatile-rich melts in channels beneath the volcanic lineaments is high and involves 10s of thousands of km<sup>3</sup>/Ma. Since mantle plumes account for more than half of the melt production at MORs our findings have important implications for our understanding of deep Earth volatile cycling.

© 2018 The Authors. Published by Elsevier B.V. This is an open access article under the CC BY license (<http://creativecommons.org/licenses/by/4.0/>).

## 1. Introduction

The eruption of basalts along the global mid-ocean ridge (MOR) system represents a major avenue for outgassing of volatiles (e.g. CO<sub>2</sub>, H<sub>2</sub>O) from the mantle (Dixon et al., 2002, 2017;

\* Corresponding author.

E-mail address: [sally@esc.cam.ac.uk](mailto:sally@esc.cam.ac.uk) (S.A. Gibson).

<sup>1</sup> Now at: Department of Earth and Space Sciences, University of Washington, 15th Avenue NE, Seattle, WA, USA.

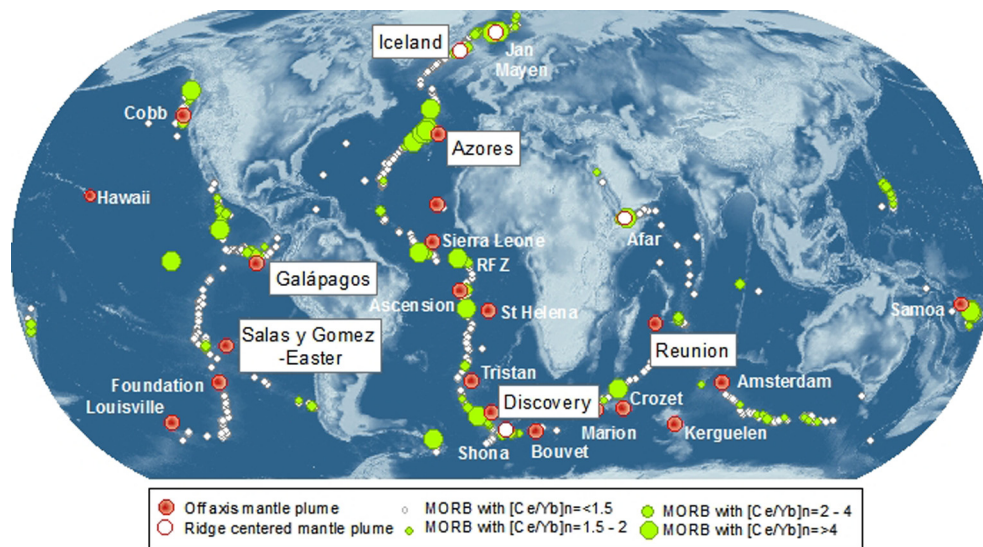


**Fig. 1.** Global distribution of MORB with elevated chondrite normalized Ce/Yb ratios. Many of the ridge segments with enriched MORB are in the vicinity of mantle plumes. Ce/Yb ratios exhibit a positive correlation with H<sub>2</sub>O but the precise relationship varies for different sites of plume–ridge interaction (see Fig. 2). The locations of hotspots discussed in the text are shown in boxes. MORB data are from Gale et al. (2013a) and Jenner and O'Neill (2012). (For interpretation of the references to colour in this figure legend, the reader is referred to the web version of this article.)

Saal et al., 2002; Simons et al., 2002; Le Voyer et al., 2015; Michael and Graham, 2015). Melt production and geochemical enrichment along MORs is not, however, uniform and varies over distances of 10s of km, e.g. Ito et al. (2003), Jenner and O'Neill (2012), Gale et al. (2011, 2013b) (Fig. 1). Some of the most convincing evidence that this variation is linked, at least in part, to melt contributions from deep-sourced mantle plume material is provided by the occurrence of high <sup>3</sup>He/<sup>4</sup>He basalts on spatially-confined sections of the global ridge system (Poreda et al., 1993; Sarda et al., 2000; Graham, 2002; Graham et al., 2014). Melting of this enriched plume material significantly affects bathymetry and basalt geochemistry along approximately 30% of the global mid-ocean ridge system (Ito et al., 2003); for hotspots such as Tristan, Azores, Easter–Salas y Gómez, Iceland and Galápagos (Fig. 1) the average flux of deep-sourced, volatile-rich material to the adjacent MOR is considerable ( $\sim 2.2 \times \text{km}^3/\text{a}$ ) and amounts to almost half of global ridge melt production (Ito and Lin, 1995). This plume–ridge interaction may be sustained over 10s if not 100s of millions of years but the physical mechanisms that allow the supply of volatile-rich melts to ridges to be maintained over long time scales are poorly understood.

Most oceanic hotspots are connected to spreading centres via lateral flow of plume material, albeit sometimes with separation distances extending over 1000 km, and this may play an important role in modulating the migration of MORs (Gibson et al., 2015). In conventional models, plumes affect MORs via straight-forward solid-state flow interactions of the sheet-like, mantle-upwelling flow induced by plate spreading along a ridge, and the upwelling of the plume itself (e.g. Feighner and Richards, 1995; Ito and Lin, 1995; Ribe, 1996). For some mantle plumes the maximum horizontal spreading of enriched plume material (i.e. the waist width) extends for almost 1000 km, e.g. the Azores, Galápagos and Iceland. While model parameters such as plume–ridge separation distance, MOR spreading rate, and plume buoyancy flux all act to control this waist width in fairly obvious ways (e.g. Feighner and Richards, 1995; Ribe, 1996; Schilling, 1991), the conventional solid-state models do not, however, explain variable amounts of trace element and isotopic enrichment along sections of plume-influenced ridge. Modifications to these solid-state models have therefore included the hypothesis that the plume source material may contain streaks of enriched peridotite or pyroxenite,

which undergo partial melting at lower temperatures and higher pressures (Ito and Mahoney, 2005; Gale et al., 2013b).

An alternative to purely solid-state flow interaction models involves the lateral transport of “enriched” melts toward ridges (Stroncik et al., 2008; Stroncik and Devey, 2011; Gibson et al., 2015; Mittal and Richards, 2017). The model proposed by Gibson et al. (2015) and expanded in Mittal and Richards (2017) involves pressure-induced transport at least partially via two-phase flow along a channelised network of volatile-rich melts at sub-lithospheric depths, embedded in the plume itself, or along the base of the lithosphere, away from the plume. Evidence cited in these studies includes the correspondence of volcanic “lineaments” connecting mantle plume stems with spatially-confined enriched MORB, such as the Wolf–Darwin lineament in Galápagos.

The conceptual models that relate volcanic lineament formation between the plume and ridge to volatile-rich melt channels at sub-lithospheric depths contrast with those that invoke passive melting due to upwelling flow beneath linear lithospheric extensional structures, e.g., Sinton (2003). These extensional models are, however, inconsistent with a broad range of geophysical and geological observations. For Galápagos this evidence includes the following arguments: (1) Mapped fault orientations do not correspond to the orientations of the volcanic lineaments (Mittelstaedt et al., 2012). (2) The dominant extensional feature in the region, the Galápagos Transform Fault, shows no evidence of associated volcanism (Mittal and Richards, 2017). (3) Numerical calculations of passive upwelling suggest insufficient melt production to explain the lineament volumes (Mittelstaedt et al., 2012). (4) Gravity analysis does not indicate pervasive intrusion associated with the pattern of extension in the region (Mittal and Richards, 2017). (5) Regional seismicity is not related to the locations of the lineaments, suggesting that they do not represent primary faulting structures (Mittal and Richards, 2017). As we illustrate in detail below, enigmatic volcanic lineament structures also link other hotspots (Azores, Salas y Gómez, La Réunion and Discovery) with global spreading centres.

In this work, we examine recently published datasets for volatiles (H<sub>2</sub>O) in quenched basaltic glasses and melts trapped in olivine phenocrysts (inclusions) at archetypal regions of plume–ridge interaction. While the amount of volatile data is limited, we have been able to establish an empirical relationship between [Ce/Yb]<sub>n</sub> and H<sub>2</sub>O that we use to examine spatial variability in

H<sub>2</sub>O contents of erupted basalts. By extending rare-earth element inversion models to include volatile elements and both active and passive mantle upwelling we make the first attempt to: (i) quantify the H<sub>2</sub>O contents of melts generated “deep” in the stems of upwelling mantle plumes; and (ii) infer the patterns of melt generation and transport required to explain simultaneously the excess crust, trace element, isotopic, and volatile signatures of mantle plumes along nearby MORs.

## 2. Variability in volatile contents of plume-related MORB

Precise analyses of volatiles in submarine glassy lavas combined with olivine-hosted melt inclusions potentially yield important information on the original contents of dissolved volatiles in primary OIB and MORB melts (Hauri et al., 2006), but such analyses require rigorous filtering to remove the effects of degassing and interaction with altered oceanic crust or seawater. Here, we focus on H rather than other volatiles because of the problems of degassing associated with C and the relatively small datasets for S, F, Cl. To establish the primary H<sub>2</sub>O contents of melts generated at different sites of plume–ridge interaction, we filtered published datasets of both basaltic glasses (with MgO >6 wt.%) and melt inclusions in magnesium-rich olivine (>80% Fo) from ocean islands, seamounts and associated MORs using H<sub>2</sub>O/K<sub>2</sub>O, Cl/Nb and Cl/K<sub>2</sub>O ratios (Supplementary File 1). We then used liquid lines of descent from the most primitive basaltic glasses and melt inclusions to fractionation correct these datasets to 8 wt.% MgO (Supplementary File 2). This is the near minimum MgO content of primary MORB (referred hereafter as [H<sub>2</sub>O]<sub>8</sub>). Oceanic basalts with >8 wt.% MgO are largely associated with olivine-only crystallisation; this does not significantly impact on fractionation corrected H<sub>2</sub>O contents because of the low partition coefficient for H between olivine and basaltic melt (0.001–0.002), whereas basalts with 6 to 8 wt.% MgO have also undergone fractional crystallisation of plagioclase and clinopyroxene that have higher partition coefficients for H (0.01 and 0.023, respectively; Aubaud et al., 2004).

Hydrogen and the light rare-earth elements (LREEs) exhibit a similar, moderately-incompatible behaviour during peridotite melting and H<sub>2</sub>O/Ce ratios have widely been used to assess de- and ingassing of H in MORB and OIB. Despite filtering for secondary processes there remains, however, a considerable variability in H<sub>2</sub>O/Ce ratios of global OIB and MORB (from 50 to 315) that must reflect differences in melting processes and also source compositions, e.g. (Michael, 1995; Dixon et al., 2002, 2017; Saal et al., 2002; Le Voyer et al., 2015; Shimizu et al., 2016; Kendrick et al., 2017). Correlation matrices for sections of ridge influenced by the Azores, Galapagos, Easter–Salas y Gómez, Discovery and Réunion mantle plumes confirm the similar compatibility of H with both La and Ce ( $R^2 = 0.86$ – $0.99$  and  $0.88$ – $1.0$ , respectively; see Supplementary Table 1). They also reveal a good correlation between H<sub>2</sub>O and [Ce/Yb]<sub>n</sub> ( $R^2 = 0.76$ – $0.97$ ). This empirical relationship, which is shown graphically in Fig. 2, allows us to calculate [H<sub>2</sub>O]<sub>8</sub> contents for seamounts and volcanic islands that do not contain enough analyses to accurately calculate liquid lines of descent and correct to 8 wt.% MgO. To a first order, the empirical relationship between [Ce/Yb]<sub>n</sub> and [H<sub>2</sub>O]<sub>8</sub> remains constant for basalts with >6 wt.% MgO that are influenced by the same mantle plume (Fig. 2 and Supplementary File 2); in the remainder of the manuscript this proxy for [H<sub>2</sub>O]<sub>8</sub> is referred to as [H<sub>2</sub>O]<sub>8</sub><sup>\*</sup>. We note that at a given [Ce/Yb]<sub>n</sub> ratio the observed contents of [H<sub>2</sub>O]<sub>8</sub> are low in basalts influenced by the Réunion and Discovery mantle plumes relative to those influenced by the Azores, Galapagos and Easter–Salas y Gómez plumes. This is consistent with the presence of a so-called EM (enriched mantle) reservoir, which has been interpreted as subducted and dehydrated oceanic lithosphere (Supplementary File 1; Dixon et al., 2002, 2017).

The highest [H<sub>2</sub>O]<sub>8</sub><sup>\*</sup> contents (up to 1.3 wt.%) occur in MORB influenced by near-axis plumes, such as on the Mid Atlantic Ridge (~39°N) adjacent to the Azores hotspot and Galápagos Spreading Centre (90.5–89.53°W) near the Galápagos hotspot (Fig. 3). Slightly lower maximum [H<sub>2</sub>O]<sub>8</sub><sup>\*</sup> contents (up to 0.7 wt.%) are found in basaltic glasses associated with off-axis plumes, e.g. on the East Pacific Rise (26.8°S) at the intersection with the Easter–Salas y Gómez hotspot track; the Mid Atlantic Ridge adjacent to the Discovery hotspot (48.76°S) and on the Central Indian Ridge (18.35°S) north of the intersection of the Rodrigues Ridge, which connects the spreading centre to the Réunion hotspot.

We observe that >80% of MORB on plume-influenced ridges have up to 0.4 wt.% [H<sub>2</sub>O]<sub>8</sub><sup>\*</sup>, i.e. almost twice that of normal (N-) MORB, which has <~0.2 wt.% H<sub>2</sub>O (Danyushevsky et al., 2000; Fig. 4). The modal H<sub>2</sub>O content of plume-influenced MORB is slightly higher for those associated with near axis plumes (Azores and Galápagos) than off axis plumes (Réunion or Easter–Salas y Gómez). Plume-influenced MORB that are moderately enriched in volatiles (0.2 and 0.4 wt.% H<sub>2</sub>O) exhibit a systematic, long wave-length correlation of geochemical enrichment with increasing bathymetry (Fig. 4) and crustal thickness. Although the bathymetric peak on sections of plume-influenced ridge often coincides with the most volatile-enriched MORB (>0.4 wt.% H<sub>2</sub>O), there is no first order correlation between degree of overall geochemical enrichment and bathymetry (Fig. 4).

The empirical relationship between [Ce/Yb]<sub>n</sub> and [H<sub>2</sub>O]<sub>8</sub> for plume-influenced MORB can be extrapolated through analyses of basaltic glasses and melt inclusions from islands and seamounts located along hot spot tracks and corresponding plume stems (Fig. 2). This relationship has allowed us to construct proxy maps for H<sub>2</sub>O at different sites of plume–ridge interaction at a higher resolution than would have been possible from published H<sub>2</sub>O contents alone (Fig. 3). A striking observation from these maps is that the most H<sub>2</sub>O-rich MORB have a tendency to occur near where large volcanic lineaments radiating from mantle plume stems intersect the ridge axis. Perhaps the most impressive is on the Mid Atlantic Ridge (MAR) at 47.5–48.5°S, near its intersection with the Discovery Ridge. This relationship is also apparent where volcanic lineaments intersect the Galápagos Spreading Centre between 91 and 92.5°W, and at Menez Gwen and Lucky Strike on the MAR south of its intersection with the Azores hot spot. Fig. 3 shows that melts erupted along some of these lineaments (Wolf–Darwin, Rodrigues Ridge) also have high (H<sub>2</sub>O)<sub>8</sub><sup>\*</sup> contents. For the Rodrigues Ridge, which radiates from the Réunion plume to the Central Indian Ridge, H<sub>2</sub>O contents of erupted basalts decrease as the ridge is approached and become similar to the values of N-MORB.

## 3. Coincidence of volatile-rich MORB and elevated ridge bathymetry

The presence of volatile-rich melts on bathymetrically shallow parts of MORs presents a paradox: conventional dynamic mantle melting models predict that incompatible-trace-element enriched melts are generated by lower degrees of adiabatic decompression melting, and are hence associated with smaller melt volumes, than more depleted melts. For Galápagos, Azores and Iceland the general coincidence of enriched basalts and thick crust has been modelled as an increased flux of enriched, solid plume material into the base of the sub-ridge triangular melting regime due to buoyancy-driven active upwelling (MacLennan et al., 2001; Asimow and Langmuir, 2003; Asimow et al., 2004; Ingle et al., 2010). This solid-state interaction is able to satisfactorily account for the mean compositions of plume-influenced MORB and crustal thickness over 100s of km. Nevertheless, at short wavelengths (10s of km) along sections of ridge influenced by off axis plumes the

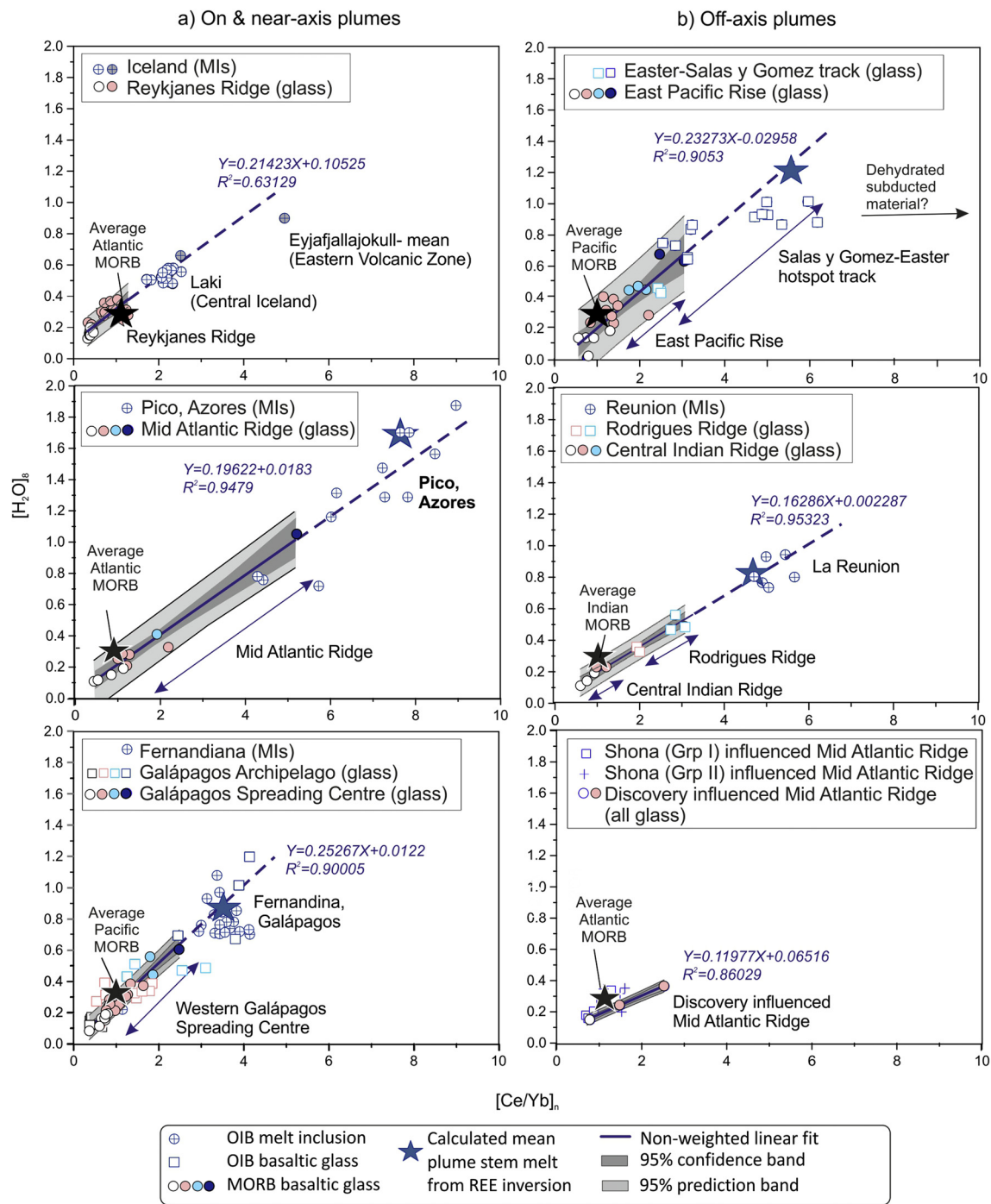


**Fig. 2.** Plots of chondrite-normalised Ce/Yb versus  $H_2O$  normalised to 8 wt.% MgO ( $[H_2O]_8$ ) for basalts from mantle plume related islands and seamounts, and adjacent mid-ocean ridges.  $H_2O$  data were filtered to remove the effects of in- and out-gassing (see Supplementary File 1 for discussion). Analyses of Fernandina submarine basaltic glasses have been excluded due to considerable H loss relative to olivine-hosted melt inclusions from the same region. Plume-influenced MORB show a strong positive correlation between chondrite-normalised  $[Ce/Yb]_n$  and  $[H_2O]_8$  and almost all analyses fall within 95% prediction bands. Data for ocean islands and seamounts fall within extrapolated 95% prediction bands for MORB. Dashed lines are extrapolations of the MORB regression lines (solid lines), except for b) where data for the Rodrigues Ridge are also included. Blue stars show the compositions of plume stem melts predicted by REE inversion models for olivine-hosted melt inclusions and glasses from La Réunion, Salas y Gómez, Fernandina and Pico (Supplementary Table 3). Data sources are as follows: Azores (Dixon et al., 2002, 2017; Gale et al., 2013a; Métrich et al., 2014); Galápagos (Cushman et al., 2004; Koleszar et al., 2009; Peterson et al., 2017); Easter (Simons et al., 2002); Iceland (Hilton et al., 2000; Murton et al., 2002; Nichols et al., 2002; Moune et al., 2012; Hartley et al., 2014); Réunion (Murton et al., 2005; Di Muro et al., 2014) and Discovery, Shona (Dixon et al., 2002). (For interpretation of the references to colour in this figure legend, the reader is referred to the web version of this article.)

enrichment of H coincides with incompatible trace element ratios, Sr, Nd and Pb isotopes but is offset from He isotopes (Simons et al., 2002; Stroncik et al., 2008; Graham et al., 2014). This decoupling of  $^3He/^4He$  from lithophile isotopic ratios has been used as primary evidence that enriched plume material is transported to the ridge as a melt rather than a solid (Stroncik and Devey, 2011).

The elevated bathymetry associated with the most-enriched plume-influenced MORB constitutes localised 'bumps' (less than  $\sim 1$  km in height) superimposed on the long wave-length bathymetric gradients. A key observation from our study is that at archetypal examples of plume-ridge interaction there is no systematic increase in melt productivity with geochemical enrich-

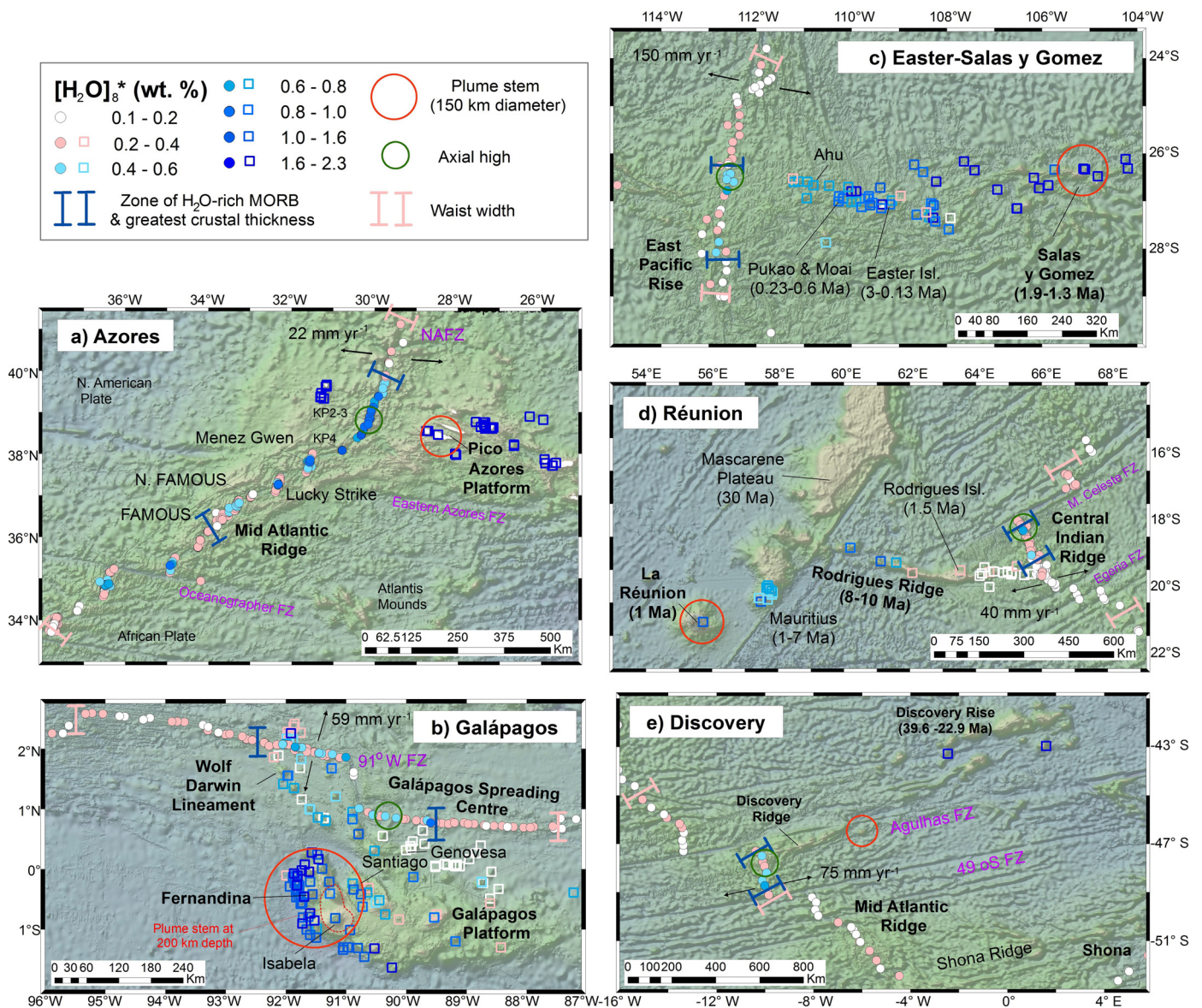


**Fig. 3.** Spatial variability in  $[H_2O]_8^*$  contents of basalts from: (a) the Azores; (b) Galápagos; (c) Easter-Salas y Gómez; (d) La Réunion; and (e) Discovery.  $[H_2O]_8^*$  is calculated using  $[Ce/Yb]_n$  as a proxy and the equations given for each location in Fig. 2. MORB are shown by closed circles and OIB by open squares. The waist width is defined by the extent of plume-influenced ridge. Data sources are: Beier et al. (2012); Christie et al. (2005); Fretzdorff et al. (1996); Gale et al. (2011, 2013b, 2013a); Harpp and White (2001); Haase et al. (1996, 1997); Hanan and Schilling (1989); Kingsley and Schilling (1998); le Roux et al. (2002a, 2002b); Jenner and O'Neill (2012); Machida et al. (2014); Mellor (1998); Nauret et al. (2006); Saal et al. (2007); Schilling et al. (2003) and those given in Fig. 2. (For interpretation of the references to colour in this figure legend, the reader is referred to the web version of this article.)

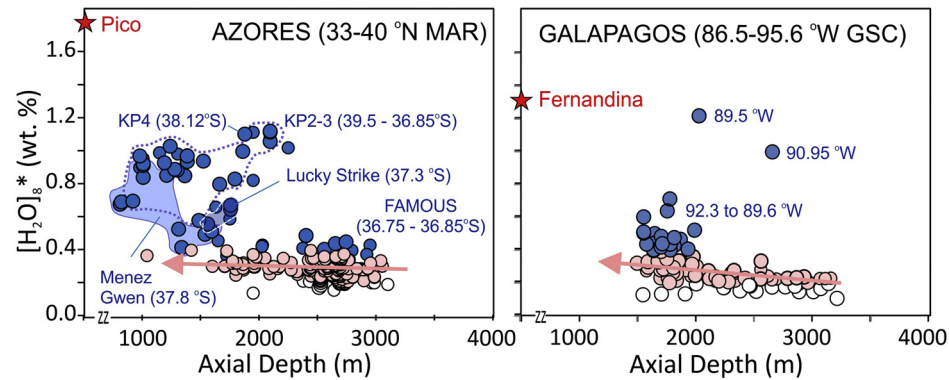
ment, i.e. contribution from the plume (Fig. 4). Moreover, at many of these locations there is considerable range in incompatible-trace-element ratios at a single isotopic composition and we agree with Gale et al. (2013b) that these features are testimony to a localised, variably-enriched melt supply. Below we use REE inversion models to explore how these punctuated anomalies at spatially-confined sites of plume-ridge interaction are controlled by melting processes, i.e. depth of melting, H contents of contributing mantle source regions and the relative flux of enriched material into the melting region.

#### 4. Constraints on plume-ridge interactions using REE inversion melting models

Basalts from sections of the global ridge system that are influenced by mantle plumes are characterised by strong enrichments in light rare-earth elements (La, Ce, Pr, Nd, Sm) that give rise to

sharp inflections on normalised plots (Fig. 5a). These enrichments cannot be modelled by single-stage melting of the MORB source and are testimony to the involvement of more complex mantle processes. The INVMEL (inversion melting) algorithm of McKenzie and O'Nions (1991) was designed to simultaneously model concentrations of all of the REEs and non-volatile elements in mantle melts and predict variations in melt fraction with depth during adiabatic decompression. Previous REE inversion models for N-MORB have incorporated the passively-driven, corner-flow solution and have been able to satisfactorily reproduce the observed concentrations of REEs and other trace elements in MORB in regions of plume-ridge interaction, but they significantly underestimate the crustal thicknesses as determined by seismic studies (e.g. Iceland; MacLennan et al., 2001). The REE inversion program of McKenzie and O'Nions (1991) now incorporates algorithms that more appropriately describe both active and plate-driven passive upwelling melting regimes. INVMEL has also been modified to in-

## a) Near axis plumes



## b) Off axis plumes

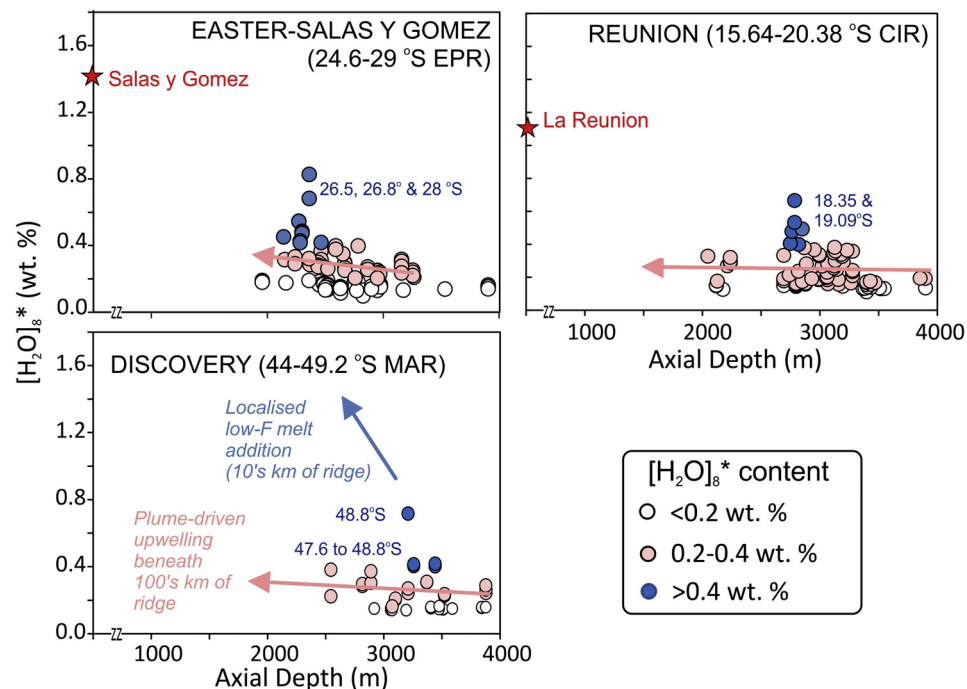


**Fig. 4.** Depth versus  $[\text{H}_2\text{O}]_8^*$  for plume-influenced MORB. Pink arrows are based on regression lines through the datasets for MORB with moderate  $\text{H}_2\text{O}$ . Note the different correlations for MORB with moderate  $\text{H}_2\text{O}$  (0.2–0.4 wt.%; pink circles) and high  $\text{H}_2\text{O}$  contents (>0.4 wt.%; blue circles). This difference in melt productivity with volatile content implies that different processes are involved in their formation. The highest concentration of  $\text{H}_2\text{O}$  in corresponding plume stem melts (red star) is shown for reference. Data sources are as in Fig. 3. (For interpretation of the references to colour in this figure legend, the reader is referred to the web version of this article.)

clude mineral-melt partition coefficients and source concentrations of volatile elements (see Supplementary File 3).

In our REE inversion models we use published concentrations of volatile and non-volatile elements for samples with >6 wt.% MgO and collected: (i) immediately above the postulated locations of present-day, near- and off-axis plume stems; and (ii) on the adjacent section of ridge (Figs. 6 and 7). Our models assume that the erupted basalts sample the entire melting region and instantaneous melts derived from small-scale lithological or compositional heterogeneities in the mantle are homogenised during transport. We follow the findings of previous work and assume that: (i) the isotopically depleted component associated with plume-influenced MORB near the Azores, Galapagos, Reunion, Easter–Salas y Gómez and Discovery is intrinsic to the mantle plume itself; (ii) primitive mantle is the dominant enriched  $^{143}\text{Nd}/^{144}\text{Nd}$  component; and (iii) recycled lithosphere constitutes a relatively minor contribution (Douglass et al., 1999; Sarda et al., 2000; Dixon et al., 2002, 2017; Simons et al., 2002; Schilling et al., 2003; Ingle et al., 2010; Füre et al., 2011; Gibson et al., 2015).

While the results of REE inversion are non-unique and model dependent, we attempt to constrain these using the findings of experimental and analytical studies. Experiments indicate the anhydrous peridotite solidus is intersected at a depth of  $\sim 60$  km at ambient mantle potential temperatures ( $T_P = 1315$  °C) and increases to 80–120 km at the elevated  $T_P$  associated with mantle plumes (Hirschmann et al., 2009). Despite being present at only trace concentrations, excess  $\text{H}_2\text{O}$  has a disproportionately large effect on the melting behaviour of the mantle (Asimow and Langmuir, 2003; Asimow et al., 2004). For the small amounts of water present in the MORB source, incipient wet melting at ambient  $T_P$  will occur at a depth of  $\sim 120$  km (Asimow et al., 2004). At the very high volatile contents (900 ppm  $\text{H}_2\text{O}$ ) and higher mantle potential temperatures inferred for some mantle plumes 1% melting is estimated to occur at depths  $\sim 180$  km (Novella et al., 2014). On melt fraction versus depth plots these small melt fractions are represented by a low-productivity “tail” below the anhydrous peridotite solidus (Fig. 8). Here, we use concentrations of the highly-incompatible trace elements (Cs, Rb, Ba, U and Th) to predict the onset of melt-

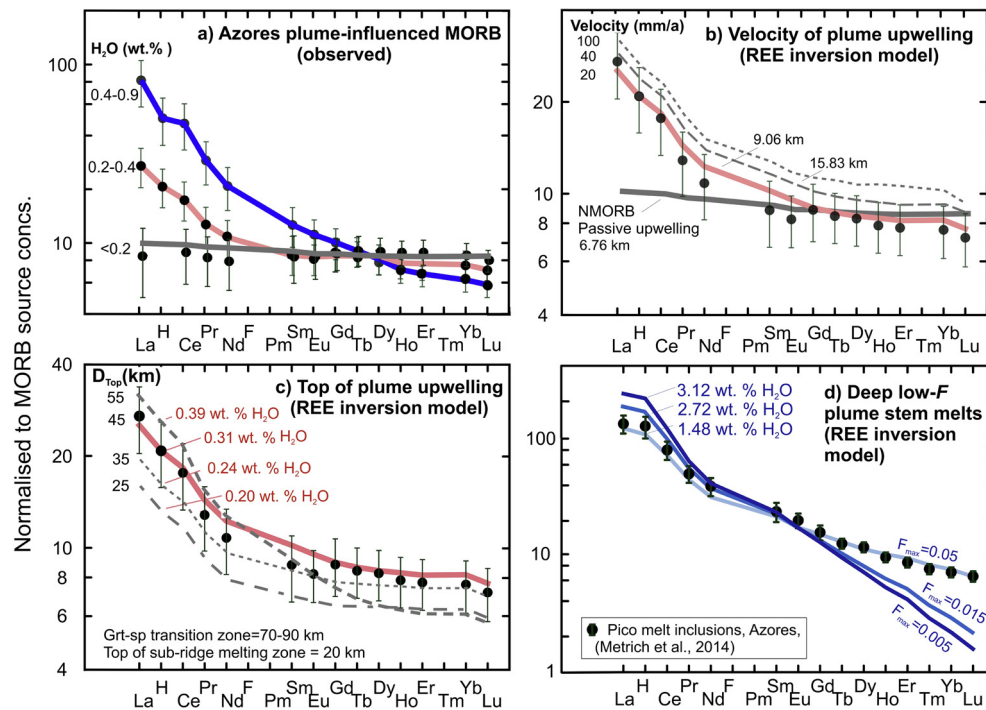


**Fig. 5.** a) Comparison of rare-earth element patterns of MORB from the Mid Atlantic Ridge (33–40°N) in the region influenced by the Azores mantle plume. Closed circles are for mean observed concentrations and vertical bars show the standard deviation. b) Results of one-dimensional synthetic REE inversion models designed to simulate solid-state flow interaction between buoyant plume material and advection of upper mantle material by the spreading ridge. Closed circles are for mean observed concentrations of MORB with 0.2 to 0.4 wt.% [H<sub>2</sub>O]<sub>0</sub>. Melt thickness is given in km. c) Effects on REE patterns of varying the top of the zone of active plume upwelling from 55 to 25 km. Depths (in km) denote the upper limit of active plume upwelling in a melt column with a top boundary set at 18 km. d) Results of one-dimensional synthetic REE inversion models designed to simulate deep melting in an upwelling mantle plume stem. Closed circles are the mean observed concentrations of olivine-hosted melt inclusions and bulk-rock data from Pico, Azores (Métrich et al., 2014). (For interpretation of the references to colour in this figure legend, the reader is referred to the web version of this article.)

ing. This is because these elements strongly partition into the melt during the deepest melting and will be potentially ‘stripped’ from the mantle residue together with rare gases (He, Ar), followed at progressively shallower depths by H and the light REEs (La, Ce; Fig. 8).

Under mantle conditions the greatest influence on the concentrations of H and the light REEs is the amount of pyroxene melting whereas the main control on the concentrations of heavy REEs is melting of garnet. Heavy REEs (such as Yb) become progressively more concentrated as the increasingly refractory mantle upwells into the spinel stability field. Since the depth of garnet stability in the mantle is temperature dependent (Klemme and O’Neill, 2000), we set the garnet–spinel reaction zone at 60 to 80 km for melting of ambient mantle, 70 to 90 km for plume-influenced ridge and 80 to 100 km for melting in mantle plume stems.

## 5. Application of revised REE inversion techniques to global sites of plume–ridge interaction

We evaluated the results of our REE inversion models from the misfit between: (i) predicted and observed concentrations of REEs and other trace elements; (ii) calculated and measured melt water contents; and (iii) calculated melt thicknesses compared with seismically determined ocean crustal thickness. In almost all of our preferred models the predicted concentrations of volatile and non-volatile elements are within uncertainty of the observed data and the melt thicknesses are consistent with seismic data (Supplementary Figs. 1 and 2; Supplementary File 3).

### 5.1. “Standard” solid-state plume–ridge interaction model

Initially, our REE inversion models were formulated to simulate the “standard” plume–ridge interaction model that involves

melting of buoyant mantle plume material beneath a mid-ocean ridge (Fig. 9). These models mix the predicted compositions of melts generated by active upwelling in a sheet of mantle with those generated by passive melting in the overlying melting region. We first ran multiple iterations of synthetic melt models, based on the compositions of basalts from the MAR adjacent to the Azores hotspot (Fig. 5a), to establish how the concentrations and ratios of REEs, and also crustal thickness, are influenced by (i) plume upwelling velocity and (ii) depths of active and passive upwelling. Our results show that a decrease in the velocity of mantle material upwelling into the melting zone causes only a slight decrease in REE concentration but has a major effect on the overall thickness of crust that is generated (Fig. 5b). More critical is the depth of the top of the zone of active upwelling; as this decreases the REE patterns of the melts become flatter, approaching those of N-MORB, and the corresponding amount of crust generated increases dramatically (Fig. 5c). These findings are consistent with those of Asimow and Langmuir (2003) but our models are an advance on this earlier work because they account for variations in ratios and concentrations of all of the REEs, H<sub>2</sub>O and also other incompatible trace elements.

Following these synthetic tests we then inverted the REE concentrations of moderately-enriched MORB, with 10–40 times the MORB source concentrations of LREEs and 0.2–0.4 wt.% H<sub>2</sub>O; basalts with these compositions are ubiquitous along the whole waist width of plume-influenced ridges (Fig. 3). Our REE inversion models show that, while passive upwelling of primitive mantle can generate the observed compositions of moderately-enriched plume-influenced MORB, this process cannot simultaneously produce oceanic crust that is thicker than normal, i.e. greater than 7 km. By increasing the flux of primitive mantle material into the lower part of the melting region we are able to reproduce

## MORB influenced by near-axis mantle plumes

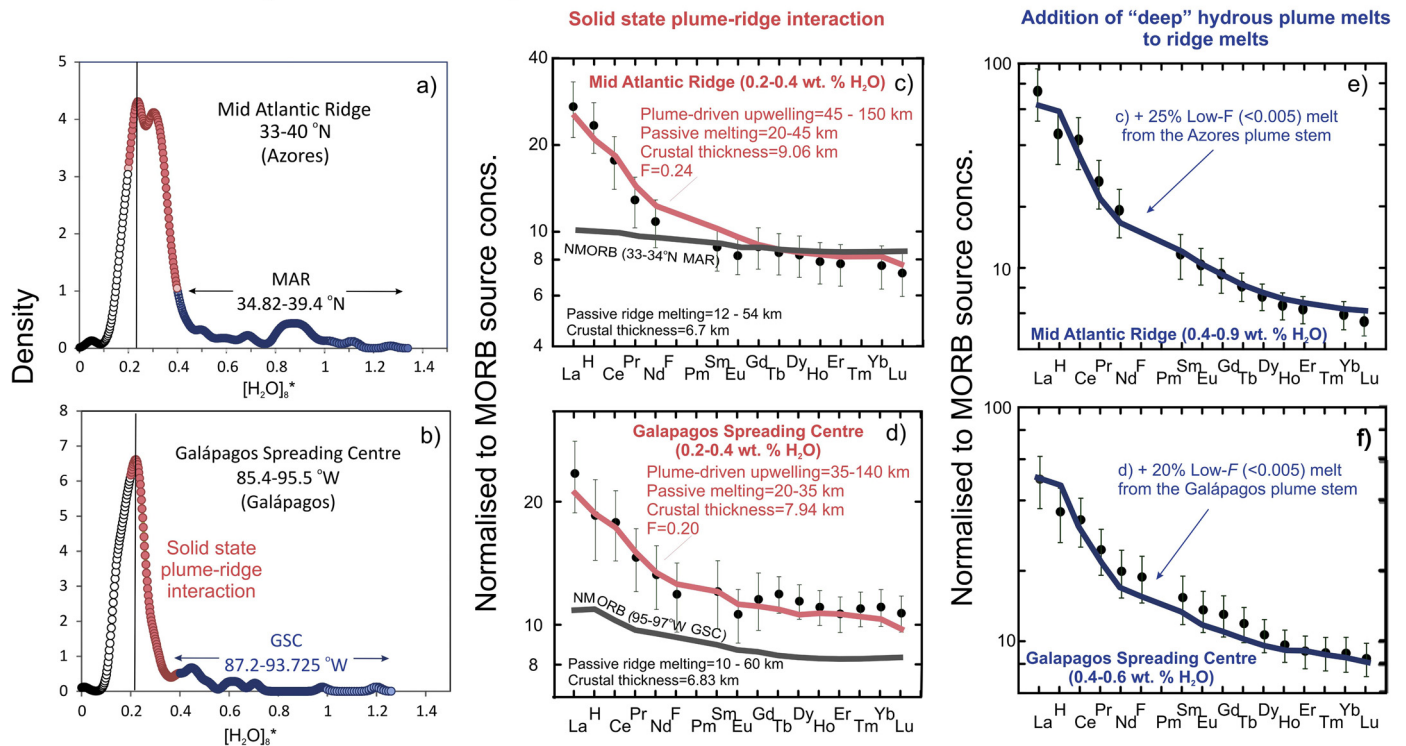


**Fig. 6.** a) and b) Kernel density plots illustrating the variation in  $[H_2O]_8^*$  contents on sections of MOR associated with near-axis plumes (Azores and Galápagos). At both locations the bulk of basalts have  $[H_2O]_8^*$  contents <0.4 wt.% and those with 0.4 to 1.2 wt.% are much less frequent. Closed circles are for mean observed concentrations and vertical bars show the standard deviation. Plots c) and d) show the best fits of REE inversion models for MORB with 0.2–0.4 wt.%  $[H_2O]_8^*$ . In order to generate the observed crustal thickness the models required mixing of melts formed by both deep active and shallow passive upwelling of plume material beneath the ridge. Plots e) and f) show the best fits of REE inversion models to MORB with 0.4–1.2 wt.%  $[H_2O]_8^*$ . These involved mixing Low- $F$  melts formed deep within the plume stem with those formed by deep-active and shallow-passive upwelling beneath the ridge shown in c) and d). The concentrations of REEs and H in N-MORB are shown for comparison in c) and d). Data sources are: Christie et al. (2005); Cushman et al. (2004); Gale et al. (2011, 2013b, 2013a); Ingle et al. (2010); Koleszar et al. (2009); Metrich et al. (2014); Schilling et al. (2003). (For interpretation of the references to colour in this figure legend, the reader is referred to the web version of this article.)

both the enriched basalt geochemistry and mean excess crustal thickness ( $\sim 1$ – $2$  km) observed at MOR segments influenced by the Azores, Galápagos, Réunion and Easter–Salas y Gómez mantle plumes (Figs. 6 and 7).

The REE inversion melt models that gave the best fit to moderately-enriched MORB influenced by the Azores, Galápagos, Réunion and Easter–Salas y Gómez mantle plumes indicate a maximum melt fraction ( $F$ ) of  $\sim 0.25$  (Fig. 8a and Supplementary Figs. 1 and 2). In order to account for the observed concentrations of HREEs in these basalts our models show that melts derived from: (i) active plume upwelling over a depth interval between 150 km to 35 km and (ii) plate-driven, passive melting of plume material at shallower depths beneath the ridge axis are required (Figs. 6 and 7). If the mantle plume is allowed to upwell further, the REE signature of melts derived from the garnet stability-field is diluted and the REE patterns are much flatter (Fig. 5a) than those actually observed.

A primary observation from our REE inversion modelling is that beneath the ridge, approximately 60% of H is exhausted from upwelling plume mantle over a 30 km depth interval below the anhydrous peridotite solidus, i.e. at depths  $>60$  km (Fig. 8b). This dehydration would increase mantle viscosity and decrease the buoyancy-driven flow of plume material into the melting region. At depths  $<35$  km upwelling of dehydrated mantle is entirely passive and governed by plate spreading of the oceanic plates (Fig. 8b). While it is beyond the scope of this work to model how the plume-derived melts would escape and react with those from the overlying passive melting region, we note that this transition region between active and passive upwelling is above the anhydrous solidus. According to the recent thermodynamic models of passive

upwelling and MORB genesis by Keller and Katz (2016) at depths of  $\sim 80$  km volatile-rich and relatively Si-poor melts trigger the formation of reactive dissolution channels and by depths as shallow as 35 km these channels are extensive. Given the increased volatile content of deep melts in regions of plume–ridge interaction these dissolution channels would be more extensive and may act as highly effective pathways for the upward migration of relatively low-viscosity enriched melts.

For all of the regions that we studied, the motion of the overlying plate and plate separation rate are relatively well-constrained and we use the best fit to the observed crustal thickness at the ridge to compute the maximum upwelling velocity in the plume (Supplementary File 3). We estimate that the average rate of active upwelling beneath the various sections of plume-influenced ridges studied here ranges from 20 to 40 mm/a at the Azores and Galápagos to 260 mm/a for Easter–Salas y Gómez. These estimates of mantle plume upwelling beneath spreading ridges are within the range calculated for plate-driven upwelling ( $\sim 10$  mm/a) and active upwelling in mantle plume stems (100s mm/a; Bourdon et al., 2006).

### 5.2. Punctuated delivery of “deep” hydrous plume melts to ridge: two-phase flow model

Although the REE inversion model for “standard” solid-state plume–ridge interaction described above satisfactorily reproduces the most highly-enriched compositions of plume-influenced MORB, the top of the melting region is required to be much deeper in order to explain the fractionated HREE ratios together with the elevated concentrations of LREEs, H (and other strongly incompatible

## MORB influenced by off-axis mantle plumes

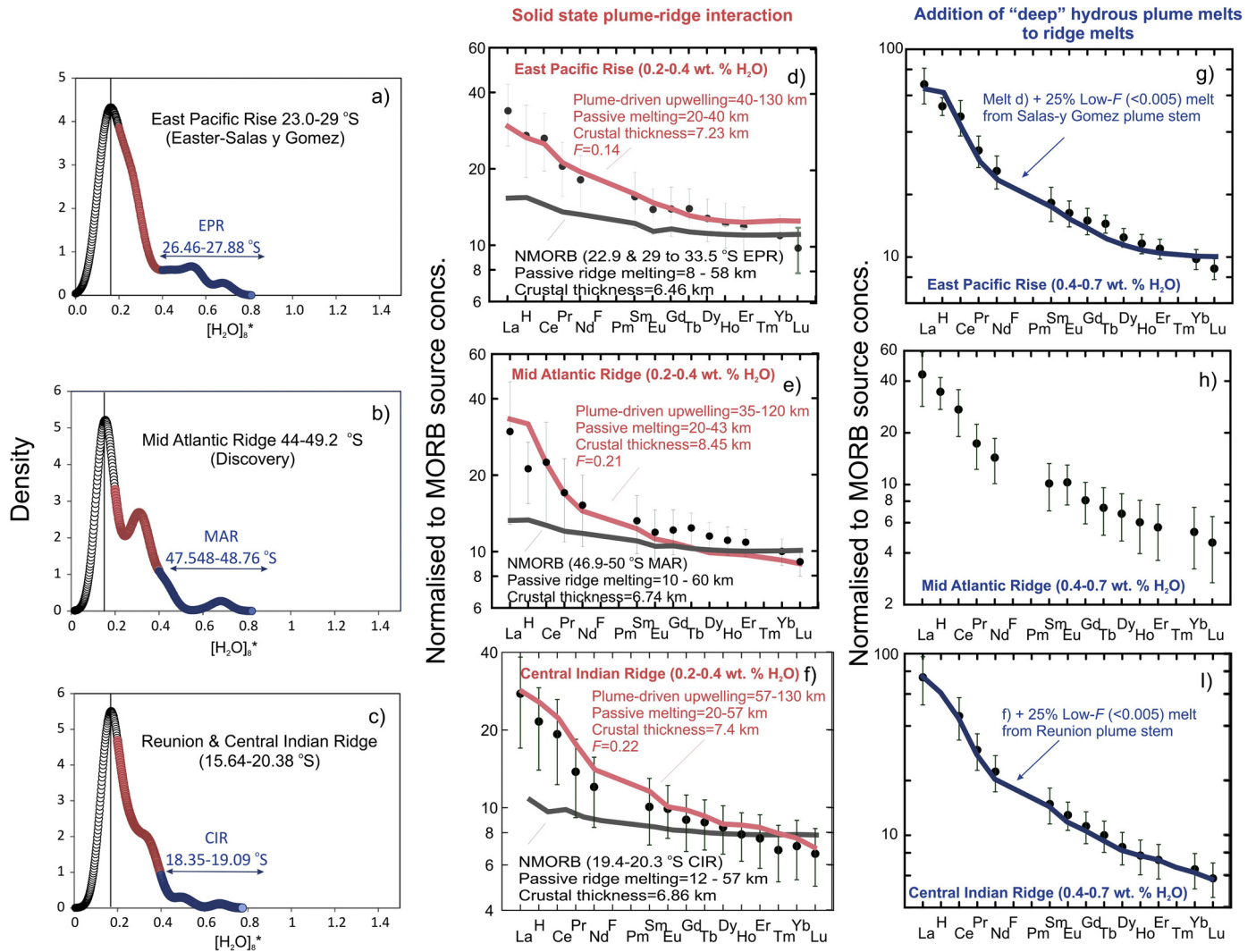


**Fig. 7.** a), b) and c) Kernel density plots illustrating the variation in  $[H_2O]_8^*$  contents on sections of MORB associated with archetypal off-axis mantle plumes (Easter-Salas y Gómez, Discovery and Reunion). At these locations the bulk of MORB have  $[H_2O]_8^*$  contents  $<0.4$  wt.% and those with  $0.4$  to  $0.8$  wt.% are much less frequent. Closed circles are for mean observed concentrations and vertical bars show the standard deviation. Plots d), e) and f) show the best fits of REE inversion models to MORB with  $0.2$ – $0.4$  wt.%  $[H_2O]_8^*$ . In order to generate the observed crustal thickness the models required mixing of melts formed by both deep active and shallow passive upwelling in the “puddle” of plume material beneath the ridge. Plots g), h) and i) show the best fits of REE inversion models to basalts with  $0.4$ – $0.8$  wt.%  $[H_2O]_8^*$ . These models involved mixing melts formed deep within the plume stem with those formed by deep-active and shallow-passive upwelling beneath the ridge (as shown in d), e) and f)). The concentrations of REEs and H in N-MORB are shown for comparison in d), e) and f). Data sources are: Douglass et al. (1999); Murton et al. (2002, 2005); le Roux et al. (2002a, 2002b); Simons et al. (2002). (For interpretation of the references to colour in this figure legend, the reader is referred to the web version of this article.)

trace elements) displayed by these basalts (Fig. 5d). It is, however, difficult to envisage why a very large increase in the depth of the top of the melting region might occur over the short length scales (10s of km) at which these highly-enriched basalts are found at different spreading ridges (Fig. 3). This small-scale variation has previously been attributed to localised, deep melting of km scale ‘blobs’ of enriched material (Ito and Mahoney, 2005) or rafts of delaminated metasomatised lithosphere (Gale et al., 2013b) but it is not straightforward to reconcile how such processes might be sustained beneath the same location, and at the relatively long timescales (millions of years) required to explain the generation of similarly-enriched melts found on the volcanic lineaments that connect the sites of volatile-rich MORB generation to plume stems (Table 1 and Fig. 3).

While plume-influenced MORB with  $>0.4$  wt.%  $H_2O$  occur at all the archetypal sites of plume-ridge interaction investigated here they are far less abundant than MORB with lower  $H_2O$  contents (Figs. 6 and 7). An elevated plume flux at a constant

plate separation rate would significantly increase crustal thickness but for individual sites of plume-influenced MORB the most highly-enriched and moderately-enriched basalts occur at similar axial depths (Fig. 4). The lack of evidence for a dramatic increase in crustal thickness at these locations implies that the processes involved in the generation of spatially-confined, highly-volatile-enriched MORB (with  $H_2O$  contents  $>0.4$  wt.%) are different to those associated with more widespread, moderately-enriched plume-influenced MORB ( $0.2$ – $0.4$  wt.%  $H_2O$ ).

Motivated by the coincidence of volatile-rich MORB and volcanic lineaments radiating from mantle plumes (Fig. 3) we focused on the effects of adding melts from the plume stem to those generated by solid-state interaction between buoyant plume material and the MOR (Fig. 9). The most successful of our models are those that simulate mixing of “deep” Low-F ( $<0.005$ ) melts from plume stems with those from solid plume material upwelling beneath the ridge (Figs. 6e, f and 7g, h, i). We used the INVMEL code to calculate the compositions of melts formed “deep” in the stems of indi-

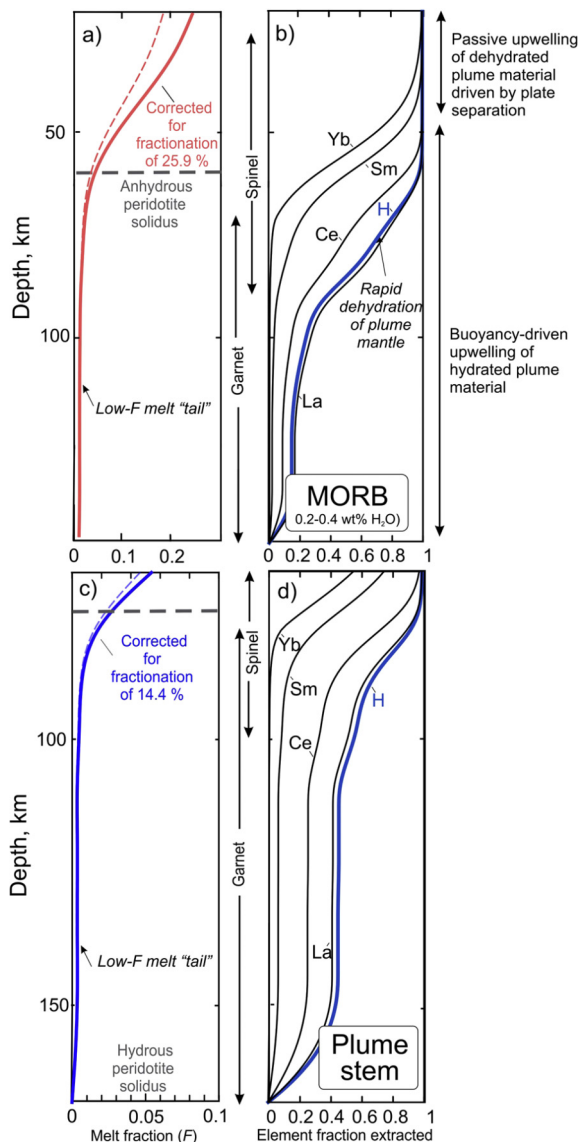


**Fig. 8.** Variation of: (a) Melt fraction versus depth for MORB with 0.2–0.4 wt.% H<sub>2</sub>O formed by during adiabatic decompression melting during deep active and shallow passive upwelling of solid plume material beneath the ridge. (b) Fraction of La, H, Ce, Sm and Yb extracted from the mantle during melting. Note the rapid dehydration of upwelling mantle immediately below the anhydrous peridotite solidus. (c) Melt fraction with depth during adiabatic decompression melting for plume stem melts. (d) Fraction of La, H, Ce, Sm and Yb extracted from the mantle during melting in the Azores plume stem. Rapid dehydration of the source is predicted between 90 and 80 km. Data used in the models are for: (a) and (b) analyses of basaltic glasses from 33–40°N on the MAR (Gale et al., 2011, 2013a, 2013b); and (c) and (d) olivine-hosted melt inclusions from Pico, Azores (Métrich et al., 2014). (For interpretation of the references to colour in this figure legend, the reader is referred to the web version of this article.)

vidual plumes (e.g. Fig. 5d). We subsequently mix these melts with those formed by solid-state interaction between buoyant mantle plume material and shallow passive upwelling beneath the ridge (as described in Section 5.1 above). The best fits to the geochemistry of the highly-enriched MORB require that plume stem melts are formed by melting between depths of 160 km and 90 km. Because the upper boundary of the Low-F melt zone is well within the garnet stability field, these Low-F (<0.005) ‘deep’ plume stem melts have relatively low concentrations of heavy REEs (e.g. Yb) and high contents of strongly-incompatible trace elements, (e.g. H and light REEs, Fig. 5d). Assuming that the plume source has moderate water contents (~330 ppm H<sub>2</sub>O or 37 ppm H), we calculate that concentrations of H<sub>2</sub>O in adiabatic decompression melts

formed in the plume stem below 90 km are very high and may reach >3 wt.% (3350 ppm H). The relative contribution of melts generated from upwelling of solid material beneath the ridge and deep within the plume stem are similar for the different global sites of plume–ridge interaction. The contribution of the Low-F deep plume stem melts is between 20% and 25% (Figs. 6e, f and 7g, h, i). Homogenisation of these low-viscosity melts, and their channelised ascent in relative isolation from shallower melts, would preserve their geochemical signatures. (We note that as deep melting begins to occur heat will flow into the initial, hydrous melting domains, enhancing melting there – a second-order effect that is beyond the scope of our modelling work here.)

We note le Roux et al. (2002a, 2002b) similarly proposed that deep Low-F plume stem melts were responsible for highly-enriched MORB on the Southern MAR adjacent to the Discovery hotspot (Fig. 3). The fundamental difference between this model and the two-phase flow model proposed here is that we do not require the melts to solidify (i.e. form garnet pyroxenite veins) before they reach the ridge. Our interpretations are strongly influenced by the first order observation that the eruption sites of highly-enriched MORB are associated with long-lived volcanic lineaments radiating from plume stems (Fig. 3), and that melt channels connecting plume stems and MORs may be maintained in the mantle over a 1000 km in length (Mittal and Richards, 2017).

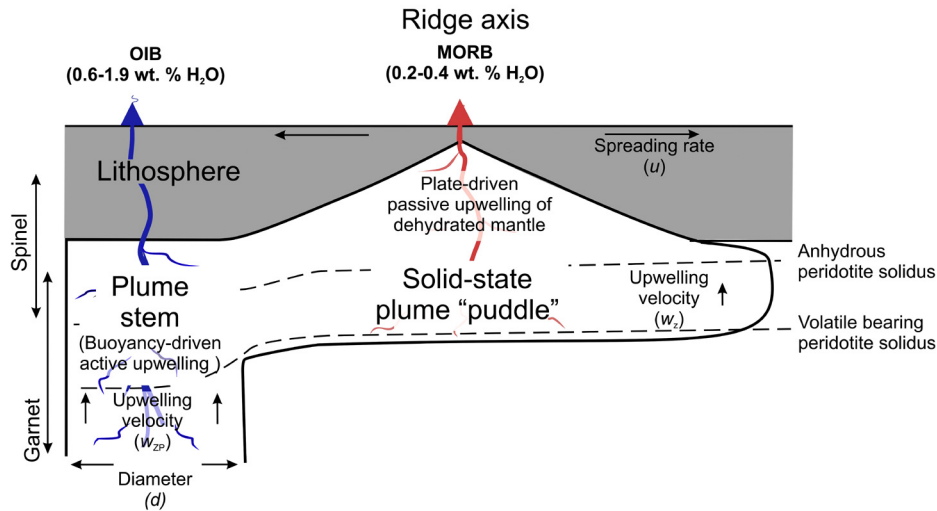
## 6. Conceptual model for a channelised magma flux from plume to ridge

Our REE inversion models are consistent with plume–ridge interaction occurring via a bimodal transport system involving: (1) ‘Classical’ solid-state flow interaction that carries volatile-bearing buoyant plume material toward the ridge, driven by the pressure gradient (Fig. 9a). This process is responsible for the large ‘waist width’ on the ridge; and (2) Rapid delivery of low-viscosity, volatile-rich melts – generated by deep, active upwelling in the plume stem – via a sub-lithospheric network of melt-rich channels. At the intersection with the ridge, melts transported in these channels cause heightened geochemical enrichment (including high-volatile (H<sub>2</sub>O) signatures), and excess crustal thickness anomalies, all above the ‘background’ signatures generated by incorporation of plume source material advected by the solid-state flow interaction process (Fig. 9b).

The model we propose is that of pressure-driven transport of low-viscosity, volatile-rich magmas from the deep plume stem toward adjacent MORs in ‘tube-like’ channels, the largest of which likely underlie the volcanic lineaments and ‘leak’ magmas through the young overlying oceanic lithosphere toward the surface along their traces. A key observation from the proxy maps shown in Fig. 3 is that basalts erupted along these long-lived volcanic lineaments contain elevated H<sub>2</sub>O contents. This is corroborated by published volatile data for basalts on the Rodrigues Ridge (Mellor, 1998), prominent lineaments in Galápagos (Peterson et al., 2017) and the more diffuse ridges that form the Easter–Salas y Gómez hotspot track (Simons et al., 2002). We anticipate that the deep volatile-rich melts are more readily able to follow established melt channels via pressure-gradient flow than higher-viscosity melts produced above the dry solidus. Our conceptual model is distinct from: (i) Braun and Sohn (2003) who modelled sheet-like transport of melt along the base of the lithosphere from plume to ridge, but did not associate the lineament structures with this distributed flow; and (ii) Morgan’s (1978) original idea of solid-state channelisation of plume flow toward the ridge, which has now been largely discounted, because the formation of such channels appears implausible from a fluid-mechanical standpoint (Sleep, 2008).

The melt-rich channels involved in plume–ridge interaction are likely established at a time when the plume is much closer to

## a) Solid-state-flow interaction



## b) Punctuated delivery of “deep” hydrous melts to ridge (two-phase flow)

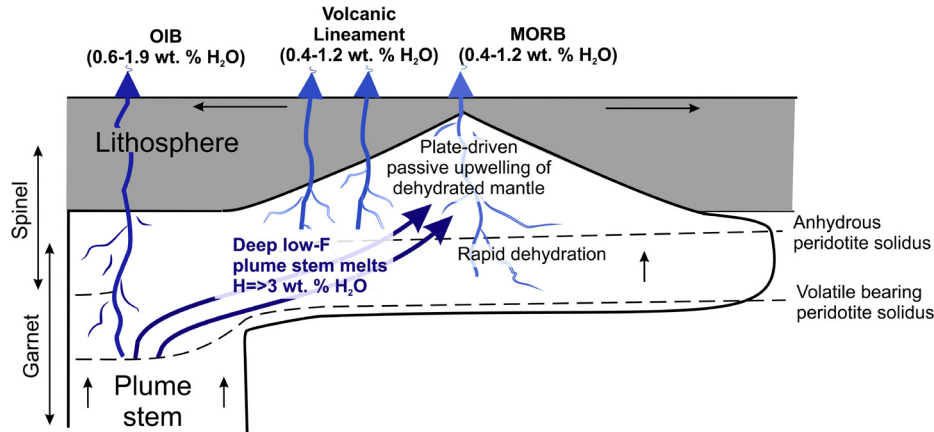


**Fig. 9.** Schematic illustrations showing the two parallel transport mechanisms involved during the interaction of near and off-axis mantle plumes with a mid-ocean ridge. (a) illustrates the “standard” solid-state flow plume–ridge interaction model and involves components of both active and passive melting beneath the ridge. (b) shows how channelised flow of deep volatile-rich plume stem melts might be superimposed on the “standard” model. In order to account for the localised occurrences of H-rich MORB and their spatial coincidence with volcanic lineaments radiating out from mantle plume stems a punctuated delivery mechanism is required. Note that the volcanic lineaments do not traverse the sub-ridge melt region, which suggests that pressure-induced channelised melt transport may have been established during transition from an on-axis to an off-axis plume (Gibson et al., 2015). The concentrations of H in the different source regions were determined from the best fit to H in REE inversion models (see text for discussion).

**Table 1**

Characteristics of volcanic lineaments radiating from mantle plume stems to nearby ridges.

Volcanic lineament	Wolf–Darwin Lineament	Discovery Ridge	Rodrigues Ridge	Salas y Gómez seamount chain
Associated mantle plume	Galápagos	Discovery	Réunion	Easter–Salas y Gómez
Height	400–2000 m	1000–3000 m	3000–4000 m	500–3500 m
Width	10–20 km	30–50 km	40–50 km	40 km
Length	200 km	250 km	400 km	535 km <sup>a</sup>
Volume	~4,000 km <sup>3</sup>	~20,000 km <sup>3</sup>	~63,000 km <sup>3</sup>	>61,000 km <sup>3</sup>
Compensated volume	~16,000 km <sup>3</sup>	~80,000 km <sup>3</sup>	~250,000 km <sup>3</sup>	>240,000 km <sup>3</sup>
Period of emplacement	~1.8 Ma	???	<8–10 Ma	<3 Ma
Rate of emplacement	~9,000 km <sup>3</sup> /Ma	???	>25,000 km <sup>3</sup> /Ma	>80,000 km <sup>3</sup> /Ma
Buoyancy flux of associated mantle plume (Sleep, 1990)	1.0 Mg/s	0.5 Mg/s	2.0 Mg/s	3.3 Mg/s

<sup>a</sup> Composed of multiple small ridges and seamounts (Rappaport et al., 1997).

the spreading axis, and remain “rooted” to both the plume stem and ridge as it migrates, either slowly or via small jumps away from the plume (Gibson et al., 2015). Deep, small-fraction melting (beneath the dry solidus) represents approximately 30% of the total volume of melt in the stems of upwelling plumes (Fig. 8c). We hypothesise that a significant fraction of this melt is transported toward the ridge via melt channels. Some insight into this

process may be gained by considering the volumes of excess melting associated with the volcanic lineaments and crustal thickness anomalies at ridge–lineament junctions (Table 1). For Galápagos as a whole, the excess crustal volume generated in direct association with recently-active volcanic lineaments (~6,000–20,000 km<sup>3</sup>; Mittelstaedt et al., 2014; Mittal and Richards, 2017) constitutes of order 5 to 20% of the total excess crustal volume (~100,000–

150,000 km<sup>3</sup>) generated by Galápagos plume (Isabela, Fernandina Islands and surroundings) during the past ~1–2 Myrs.

For the Wolf–Darwin Lineament at Galápagos, the Discovery Ridge linking the Discovery plume to the nearby southern Mid-Atlantic Ridge, and the Rodrigues Ridge linking the Réunion hotspot to the Central Indian Ridge, the associated excess crustal volumes can be estimated from the products of their approximate lengths, widths, and average heights, yielding, respectively ~4,000 km<sup>3</sup>, 20,000 km<sup>3</sup>, and 63,000 km<sup>3</sup> (Table 1). Assuming isostatic compensation, these translate into total excess crustal volumes of 16,000 km<sup>3</sup>, 80,000 km<sup>3</sup>, and 250,000 km<sup>3</sup>, respectively. For Galápagos (Wolf–Darwin), the time period of emplacement is approximately 1.8 Ma, and for Rodrigues (Réunion) this is <8–10 Ma. From these estimates, the rate of lineament generation is ~9,000 km<sup>3</sup>/Ma for Wolf–Darwin and ~25,000 km<sup>3</sup>/Ma for Rodrigues. By comparison, the volume of the ridges/lineaments connecting the active Easter–Salas y Gómez hotspot to the nearby East Pacific Rise (EPR) is ~61,000 km<sup>3</sup> (Rappaport et al., 1997), which for an estimated formation time of <3 Ma yields an emplacement rate of >80,000 km<sup>3</sup>/Ma for this moderately-high buoyancy flux hotspot. This implies a much higher fraction of excess melt delivery to the EPR due to this mantle plume, perhaps 2–3 times that at Galápagos or Réunion.

Although buoyancy fluxes cannot be translated straightforwardly into magma fluxes, the ratio of magma flux associated with lineament creation to plume buoyancy flux is similar for Galápagos and Réunion (Table 1). We therefore infer that, like Galápagos, the fraction of Réunion plume magma flux feeding Rodrigues Ridge is in the range of ~5–20%. This is consistent with the estimated volatile-rich magma flux. There are no age data available for Discovery Ridge but it is unlikely that it is more than ~10 Ma old, so the relative volume flux via an underlying melt-rich channel toward the ridge is probably at least as large as for Galápagos and Réunion. If Discovery Ridge, like Wolf–Darwin, is only ~2 Ma old, then it is possible that the melt-rich channel connecting the plume to the ridge is capturing most of the deep plume melt flux. The volcanic lineaments connecting the Azores hotspots to the nearby MAR are not as distinct, but the data presented above show that the associated and localised geochemical and volatile anomalies are just as pronounced.

A great deal of numerical modelling work has recently been done on the evolution of melt channels (see Keller and Katz, 2016 and references therein) but these models are in their infancy. Much more work is required to understand how: (i) such channels might initially form, and with physical formulations for reactive flow instabilities that are applicable for melt fractions exceeding ~5%; and (ii) the formation and evolution of volcanic lineaments may differ for plumes approaching and crossing ridges. Nevertheless, there is extensive observational evidence for channelisation beneath MORs from ophiolite complexes (Kelemen et al., 2000), so that the likelihood of melt-channel formation at high melt fraction beneath ridges and within hot plume stems is hardly in doubt. A full theoretical treatment of melt channelisation is not available at present. Mittal and Richards (2017) show, however, that melt channels established when the plume is in close proximity to the MOR can be maintained thermodynamically over plume–ridge separation distances of order ~1000 km or more for millions of years, and that transport times are sufficiently brief so as to account for U-series constraints (Kokfelt et al., 2005), given the magma fluxes inferred from the intrusive and extrusive volumes associated with the lineaments.

## 7. Conclusions

The interactions of mantle plumes (hotspots) and mid-ocean ridges play a fundamental role in mantle dynamics (Feighner and

Richards, 1995; Kincaid et al., 1995; Ribe, 1996) and, as we highlight here, these interactions are important to solid-Earth volatile cycles. Our study confirms that the amount of volatile extraction from the mantle during the generation of MORB varies along the global ridge system, and is greatest at sites of plume–ridge interaction.

MORB in the proximity of near axis plumes (e.g. Azores and Galápagos; Fig. 4) exhibit a greater overall enrichment in volatiles and excess bathymetry than MORB located >400 km from the global ridge system (such as Réunion, Discovery and Easter–Salas y Gómez). At individual sites of plume–ridge interaction there is no overall systematic variation in H content with bathymetry, which suggests that transport of volatile-rich material to the ridge is more complex than melting of a homogeneous “puddle” of buoyant plume material spreading beneath the plate as a gravity flow.

The most H-rich MORB are spatially confined and constitute mere bumps in the long wavelength ridge bathymetric profiles. The key observation arising from our proxy maps for H<sub>2</sub>O (Fig. 3) is that the most water-rich MORB occur near the intersections of volcanic ridges that radiate from mantle plumes. Moreover, basalts erupted along these long-lived volcanic ridges have similarly high H contents to those erupted on the ridge (e.g. Mellor, 1998; Peterson et al., 2017). These observations demand localised delivery of volatile-rich melts to the ridge via a process associated with the emplacement of the intersecting volcanic lineaments. The fact that the volcanic lineaments do not cross the ridges, whose locations are ephemeral relative to the plumes, requires the deep volatile-rich melts to be fed laterally. We believe that these are the surface expression of continuous flow structures in the underlying mantle, that are stable for millions of years and connect the plume stem to the ridge, rather than volcanoes that formed by melting of ‘blobs’ of enriched material.

In this paper we develop REE inversion models that simulate these two parallel systems responsible for transporting volatiles at sites of plume–ridge interaction. The most prevalent, or “background,” process involves solid-state interaction wherein buoyant material in the dispersing plume “puddle” influences the divergent upwelling generated by a mid-ocean ridge (Fig. 9a). We show that active plume upwelling, with mean velocities between 20 to 260 mm/a, and depths of greater than 35 km, can account for the observed excess crustal thickness and enrichment in volatiles (0.2 to 0.4 wt.% H<sub>2</sub>O) and other incompatible trace elements that occur over long wavelengths (100s of km) on the global ridge system (Figs. 6 and 7).

Our REE inversion models further show that low-*F* melts with >3 wt.% H<sub>2</sub>O are derived from deep, incipient melting within plume stems. The more volatile-rich MORB (0.4 to 1.2 wt.% H<sub>2</sub>O) are best explained by ~25% contribution from these deep melts. We attribute the generation of spatially-confined (over 10s of km) volatile-rich MORB to punctuated delivery of deep, small-fraction melts from the mantle plume stems. These melts would have a low viscosity enabling them to readily separate from their source regions and also to undergo pressure-induced transport over large distances, in narrow channels, feeding enriched melts towards the MORs (Fig. 9b). Although the effect of this transport mechanism on the global ridge system itself is localised, we estimate that the rate of emplacement of deep-sourced volatile-rich melts in a channelised network beneath the volcanic lineaments is high and involves transfer of 10s of thousands of km<sup>3</sup>/Ma. The long-term survival of these melt channels, which are likely established when plumes and ridges are in close proximity (Gibson et al., 2015), allows them to transfer deep-sourced volatiles to the MORs.

Since nearby mantle plumes are responsible for more than half of the melt production at MORs, the spatial variability in the MOR volatile flux provides fundamental constraints for theoretical models of deep Earth volatile cycling. For the examples we

have studied in this paper there is significant variability in plume–ridge interaction style, especially in terms of the morphology of the volcanic lineaments, as well as the individual plume–ridge interaction/migration histories. Thus these “natural experiments” form multiple probes of melt–channelisation under varying conditions, potentially leading to new insights into mantle magmatism, volatile transport, and the nature of various geochemical signals at both plumes and ridges.

## Acknowledgements

We are sincerely grateful to Dan McKenzie for expanding the REE inversion melting (INVMEL) code to incorporate volatile elements and active mantle upwelling. Our work on the role of volatiles during plume ridge interactions has been stimulated by discussions with numerous colleagues. In particular we express our gratitude to Matt Gleeson and Tushar Mittal, and to Kinga whose last great dive was to Darwin Isl, Galápagos. We thank Norm Sleep and an anonymous reviewer for their perceptive comments on an earlier version of the manuscript, and Tamsin Mather for editorial handling. This research was funded by NERC grant RG57434 (SAG) and NSF grant EAR#1615203 (MAR).

## Appendix A. Supplementary material

Supplementary material related to this article can be found online at <https://doi.org/10.1016/j.epsl.2018.07.028>.

## References

- Asimow, P.D., Dixon, J.E., Langmuir, C.H., 2004. A hydrous melting and fractionation model for mid-ocean ridge basalts: application to the Mid-Atlantic Ridge near the Azores. *Geochem. Geophys. Geosyst.* 5. <https://doi.org/10.1029/2003GC000568>.
- Asimow, P.D., Langmuir, C.H., 2003. The importance of water to oceanic mantle melting regimes. *Nature* 421, 815–820.
- Aubaud, C., Hauri, E.H., Hirschmann, M.M., 2004. Hydrogen partition coefficients between nominally anhydrous minerals and basaltic melts. *Geophys. Res. Lett.* 31. <https://doi.org/10.1029/2004GL021341>.
- Beier, C., Haase, K.M., Turner, S.P., 2012. Conditions of melting beneath the Azores. *Lithos* 144–145, 1–11.
- Bourdon, B., Ribe, N.M., Stracke, A., Saal, A.E., Turner, S.P., 2006. Insights into the dynamics of mantle plumes from uranium-series geochemistry. *Nature* 444, 713–717.
- Braun, M.G., Sohn, R.A., 2003. Melt migration in plume–ridge systems. *Earth Planet. Sci. Lett.* 213, 417–430.
- Christie, D.M., Werner, R., Hauff, F., Hoernle, K.A., Hanan, B.B., 2005. Morphological and geochemical variations along the eastern Galápagos Spreading Center. *Geochem. Geophys. Geosyst.* 6. <https://doi.org/10.1029/2004GC000714>.
- Cushman, B., Sinton, J.M., Ito, G., Dixon, J.E., 2004. Glass compositions, plume–ridge interaction, and hydrous melting along the Galápagos Spreading Center, 90.5°W to 98°W. *Geochem. Geophys. Geosyst.* 5. <https://doi.org/10.1029/2004GC000709>.
- Danyushevsky, L.V., Eggins, S.M., Falloon, T.J., Christie, D.M., 2000. H<sub>2</sub>O abundance in depleted to moderately enriched mid-ocean ridge magmas; Part I: incompatible behaviour, implications for mantle storage, and origin of regional variations. *J. Petrol.* 41, 1329–1364.
- Di Muro, A., Métrich, N., Vergani, D., Rosi, M., Armienti, P., Fougereux, T., Deloué, E., Arienzo, I., Civetta, L., 2014. The shallow plumbing system of Piton de la Fournaise Volcano (La Réunion Island, Indian Ocean) revealed by the major 2007 caldera-forming eruption. *J. Petrol.* 55, 1287–1315.
- Dixon, J.E., et al., 2017. Light stable isotopic compositions of enriched mantle sources: resolving the dehydration paradox. *Geochem. Geophys. Geosyst.* 18, 3801–3839.
- Dixon, J.E., Leist, L., Langmuir, C., Schilling, J.G., 2002. Recycled dehydrated lithosphere observed in plume-influenced mid-ocean-ridge basalt. *Nature* 420, 385–389.
- Douglass, J., Schilling, J.-G., Fontignie, D., 1999. Plume–ridge interactions of the Discovery and Shona mantle plumes with the southern Mid-Atlantic Ridge (40°–55°S). *J. Geophys. Res.*, Solid Earth 104, 2941–2962.
- Feighner, M.A., Richards, M.A., 1995. The fluid dynamics of plume–ridge and plume–plate interactions: an experimental investigation. *Earth Planet. Sci. Lett.* 129, 171–182.
- Fretzdorff, S., Haase, K.M., Garbe-Schönberg, C.-D., 1996. Petrogenesis of lavas from the Umu Volcanic Field in the young Hotspot Region west of Easter Island, southeastern Pacific. *Lithos* 38, 23–40.
- Füri, E., Hilton, D.R., Murton, B.J., Hémond, C., Dymont, J., Day, J.M.D., 2011. Helium isotope variations between Réunion Island and the Central Indian Ridge (17°–21°S): new evidence for ridge–hot spot interaction. *J. Geophys. Res.* 116. <https://doi.org/10.1029/2010JB007609>.
- Gale, A., Dalton, C.A., Langmuir, C.H., Su, Y., Schilling, J.-G., 2013a. The mean composition of ocean ridge basalts. *Geochem. Geophys. Geosyst.* 14, 489–518.
- Gale, A., Escrig, S., Gier, E.J., Langmuir, C.H., Goldstein, S.L., 2011. Enriched basalts at segment centers: the Lucky Strike (37°17′N) and Menez Gwen (37°50′N) segments of the Mid-Atlantic Ridge. *Geochem. Geophys. Geosyst.* 12. <https://doi.org/10.1029/2004GC000714>.
- Gale, A., Laubier, M., Escrig, S., Langmuir, C.H., 2013b. Constraints on melting processes and plume–ridge interaction from comprehensive study of the FAMOUS and North Famous segments, Mid-Atlantic Ridge. *Earth Planet. Sci. Lett.* 365, 209–220.
- Gibson, S.A., Geist, D.J., Richards, M.A., 2015. Mantle plume capture and outflow during Galapagos plume–ridge interaction. *Geochem. Geophys. Geosyst.* 16, 1634–1655.
- Graham, D.W., 2002. Noble gas isotope geochemistry of mid-ocean ridge and ocean island basalts: characterization of mantle source reservoirs. *Rev. Mineral. Geochem.* 47, 247–317.
- Graham, D.W., Hanan, B.B., Lupton, J.E., Hoernle, K.A., Werner, R., Christie, D.M., Sinton, J.M., 2014. Helium isotope variations and mantle plume–spreading ridge interactions along the Galapagos Spreading Centre. In: *The Galápagos: A Natural Laboratory for the Earth Sciences*. In: AGU Monographs, vol. 204, pp. 393–414.
- Haase, K.M., Devey, C.W., Goldstein, S.L., 1996. Two-way exchange between the Easter mantle plume and the Easter microplate spreading axis. *Nature* 382, 344–346.
- Haase, K.M., Stoffers, P., Garbe-Schönberg, C.D., 1997. The petrogenetic evolution of lavas from Easter Island and neighbouring seamounts, near-ridge hotspot volcanoes in the SE Pacific. *J. Petrol.* 38, 785–813.
- Hanan, B.B., Schilling, J.-G., 1989. Easter microplate evolution: Pb isotope evidence. *J. Geophys. Res.* 94, 7432.
- Harpp, K.S., White, W.M., 2001. Tracing a mantle plume: isotopic and trace element variations of Galápagos seamounts. *Geochem. Geophys. Geosyst.* 2. <https://doi.org/10.1029/2000GC000137>.
- Hartley, M.E., MacLennan, J., Edmonds, M., Thordarson, T., 2014. Reconstructing the deep CO<sub>2</sub> degassing behaviour of large basaltic fissure eruptions. *Earth Planet. Sci. Lett.* 393, 120–131.
- Hauri, E.H., Gaetani, G.A., Green, T.H., 2006. Partitioning of water during melting of the Earth’s upper mantle at H<sub>2</sub>O-undersaturated conditions. *Earth Planet. Sci. Lett.* 248, 715–734.
- Hilton, D., Thirlwall, M., Taylor, R., Murton, B., Nichols, A., 2000. Controls on magmatic degassing along the Reykjanes Ridge with implications for the helium paradox. *Earth Planet. Sci. Lett.* 183, 43–50.
- Hirschmann, M.M., Tenner, T., Aubaud, C., Withers, A.C., 2009. Dehydration melting of nominally anhydrous mantle: the primacy of partitioning. *Phys. Earth Planet. Inter.* 176, 54–68.
- Ingle, S., Ito, G., Mahoney, J.J., Chazey, W., Sinton, J.M., Rotella, M., Christie, D.M., 2010. Mechanisms of geochemical and geophysical variations along the western Galápagos Spreading Center. *Geochem. Geophys. Geosyst.* 11. <https://doi.org/10.1029/2009GC002694>.
- Ito, G., Lin, J., 1995. Mantle temperature anomalies along the past and paleoaxes of the Galápagos spreading center as inferred from gravity analyses. *J. Geophys. Res.* 100, 3733–3745.
- Ito, G., Lin, J., Graham, D.W., 2003. Observational and theoretical studies of the dynamics of mantle plume–mid-ocean ridge interaction. *Rev. Geophys.* 41. <https://doi.org/10.1029/2002RG000117>.
- Ito, G., Mahoney, J.J., 2005. Flow and melting of a heterogeneous mantle: 2. Implications for a chemically nonlayered mantle. *Earth Planet. Sci. Lett.* 230, 47.
- Jenner, F.E., O’Neill, H.S.C., 2012. Analysis of 60 elements in 616 ocean floor basaltic glasses: technical brief. *Geochem. Geophys. Geosyst.* 13. <https://doi.org/10.1029/2011GC004009>.
- Kelemen, P.B., Braun, M., Hirth, G., 2000. Spatial distribution of melt conduits in the mantle beneath oceanic spreading ridges: observations from the Ingalls and Oman ophiolites. *Geochem. Geophys. Geosyst.* 1. <https://doi.org/10.1029/1999GC000012>.
- Keller, T., Katz, R.F., 2016. The role of volatiles in reactive melt transport in the asthenosphere. *J. Petrol.* 57, 1073–1108.
- Kendrick, M.A., Hémond, C., Kamenetsky, V.S., Danyushevsky, L., Devey, C.W., Rodemann, T., Jackson, M.G., Perfit, M.R., 2017. Seawater cycled throughout Earth’s mantle in partially serpentinized lithosphere. *Nat. Geosci.* 10, 222–228.
- Kincaid, C., Ito, G., Gable, C., 1995. Laboratory investigation of the interaction of off-axis mantle plumes and spreading centres. *Nature* 376, 758–761.
- Kingsley, R.H., Schilling, J.-G., 1998. Plume–ridge interaction in the Easter–Salas y Gómez seamount chain–Easter Microplate system: Pb isotope evidence. *J. Geophys. Res.* 103, 24,159–24,177.
- Klemme, S., O’Neill, H.S.C., 2000. The near-solidus transition from garnet lherzolite to spinel lherzolite. *Contrib. Mineral. Petrol.* 138, 237–248.
- Kokfelt, T.F., Lundstrom, C., Hoernle, K.A., Hauff, F., Werner, R., 2005. Plume–ridge interaction studied at the Galápagos spreading center: evidence from

- $^{226}\text{Ra}$ – $^{230}\text{Th}$ – $^{238}\text{U}$  and  $^{231}\text{Pa}$ – $^{235}\text{U}$  isotopic disequilibria. *Earth Planet. Sci. Lett.* 234, 165–187.
- Koleszar, A.M., Saal, A.E., Hauri, E.H., Nagle, A.N., Liang, Y., Kurz, M.D., 2009. The volatile contents of the Galápagos plume; evidence for  $\text{H}_2\text{O}$  and F open system behavior in melt inclusions. *Earth Planet. Sci. Lett.* 287, 442–452.
- le Roux, P., le Roex, A., Schilling, J.-G., 2002a. MORB melting processes beneath the southern Mid-Atlantic Ridge (40–55°S): a role for mantle plume-derived pyroxenite. *Contrib. Mineral. Petrol.* 144, 206–229.
- le Roux, P., le Roex, A., Schilling, J.-G., Shimizu, N., Perkins, W., Pearce, N.J., 2002b. Mantle heterogeneity beneath the southern Mid-Atlantic Ridge: trace element evidence for contamination of ambient asthenospheric mantle. *Earth Planet. Sci. Lett.* 203, 479–498.
- Le Voyer, M., Cottrell, E., Kelley, K.A., Brounce, M., Hauri, E.H., 2015. The effect of primary versus secondary processes on the volatile content of MORB glasses: an example from the equatorial Mid-Atlantic Ridge (5°N–3°S). *J. Geophys. Res., Solid Earth* 120, 2014JB011160.
- Machida, S., Orihashi, Y., Magnani, M., Neo, N., Wilson, S., Tanimizu, M., Yoneda, S., Yasuda, A., Tamaki, K., 2014. Regional mantle heterogeneity regulates melt production along the Réunion hotspot-influenced Central Indian Ridge. *Geochem. J.* 48, 433–449.
- MacLennan, J., McKenzie, D., Gronvöld, K., 2001. Plume-driven upwelling under central Iceland. *Earth Planet. Sci. Lett.* 194, 67–82.
- McKenzie, D., O’Nions, R.K., 1991. Partial melt distributions from inversion of rare earth element concentrations. *J. Petrol.* 32, 1021–1091.
- Mellor, S.H., 1998. The Geochemistry and Petrology of the Rodrigues Ridge (Western Indian Ocean). Unpubl. PhD thesis. University of Greenwich. 322 pp.
- Métrich, N., Zanon, V., Creon, L., Hildenbrand, A., Moreira, M., Marques, F.O., 2014. Is the “Azores hotspot” a wet spot? Insights from the geochemistry of fluid and melt inclusions in olivine of Pico Basalts. *J. Petrol.* 55, 377–393.
- Michael, P., 1995. Regionally distinctive sources of depleted MORB: evidence from trace elements and  $\text{H}_2\text{O}$ . *Earth Planet. Sci. Lett.* 131, 301–320.
- Michael, P.J., Graham, D.W., 2015. The behavior and concentration of  $\text{CO}_2$  in the suboceanic mantle: inferences from undegassed ocean ridge and ocean island basalts. *Lithos* 236–237, 338–351.
- Mittal, T., Richards, M.A., 2017. Plume–ridge interaction via melt channelization at Galápagos and other near-ridge hotspot provinces. *Geochem. Geophys. Geosyst.* 18, 1711–1738.
- Mittelstaedt, E., et al., 2012. Multiple expressions of plume–ridge interaction in the Galápagos: volcanic lineaments and ridge jumps. *Geochem. Geophys. Geosyst.* 13. <https://doi.org/10.1029/2012GC004093>.
- Mittelstaedt, E., Soule, A., Harpp, K.S., Fornari, D., 2014. Variations in crustal thickness, plate rigidity and volcanic processes throughout the northern Galápagos volcanic province. In: *The Galápagos: A Natural Laboratory for the Earth Sciences*. In: AGU Monographs, pp. 263–284.
- Morgan, W.J., 1978. Rodriguez, Darwin, Amsterdam, ... a second type of hotspot island. *J. Geophys. Res.* 83, 5355–5360.
- Moune, S., Sigmarsson, O., Schiano, P., Thordarson, T., Keiding, J.K., 2012. Melt inclusion constraints on the magma source of Eyjafjallajökull 2010 flank eruption. *J. Geophys. Res., Solid Earth* 117, B00C07.
- Murton, B.J., Taylor, R.N., Thirlwall, M.F., 2002. Plume–ridge interaction: a geochemical perspective from the Reykjanes Ridge. *J. Petrol.* 43, 1987–2012.
- Murton, B.J., Tindle, A.G., Milton, J.A., Sauter, D., 2005. Heterogeneity in southern Central Indian Ridge MORB: implications for ridge–hot spot interaction. *Geochem. Geophys. Geosyst.* 6. <https://doi.org/10.1029/2004GC000798>.
- Nauret, F., Abouchami, W., Galer, S., Hofmann, A., Hemond, C., Chauvel, C., Dymont, J., 2006. Correlated trace element–Pb isotope enrichments in Indian MORB along 18–20°S, Central Indian Ridge. *Earth Planet. Sci. Lett.* 245, 137–152.
- Nichols, A.R.L., Carroll, M.R., Höskuldsson, Á., 2002. Is the Iceland hot spot also wet? Evidence from the water contents of undegassed submarine and subglacial pillow basalts. *Earth Planet. Sci. Lett.* 202, 77–87.
- Novella, D., Frost, D.J., Hauri, E.H., Bureau, H., Raepsaet, C., Roberge, M., 2014. The distribution of  $\text{H}_2\text{O}$  between silicate melt and nominally anhydrous peridotite and the onset of hydrous melting in the deep upper mantle. *Earth Planet. Sci. Lett.* 400, 1–13.
- Peterson, M.E., Saal, A.E., Kurz, M.D., Hauri, E.H., Blusztajn, J.S., Harpp, K.S., Werner, R., Geist, D.J., 2017. Submarine basaltic glasses from the Galapagos Archipelago: determining the volatile budget of the mantle plume. *J. Petrol.* 58, 1419–1450.
- Poreda, R.J., Schilling, J.-G., Craig, H., 1993. Helium isotope ratios in easter microplate basalts. *Earth Planet. Sci. Lett.* 119, 319–329.
- Rappaport, Y., Naar, D.F., Barton, C.C., Liu, Z.J., Hey, R.N., 1997. Morphology and distribution of seamounts surrounding Easter Island. *J. Geophys. Res., Solid Earth* 102, 24713–24728.
- Ribe, N.M., 1996. The dynamics of plume–ridge interaction 2. Off-ridge plumes. *J. Geophys. Res., Solid Earth* 101, 16195–16204.
- Saal, A.E., Hauri, E.H., Langmuir, C.H., Perfit, M.R., 2002. Vapour undersaturation in primitive mid-ocean-ridge basalt and the volatile content of Earth’s upper mantle. *Nature* 419, 451–455.
- Saal, A.E., Kurz, M.D., Hart, S.R., Blusztajn, J.S., Blichert-Toft, J., Liang, Y., Geist, D.J., 2007. The role of lithospheric gabbros on the composition of Galápagos lavas. *Earth Planet. Sci. Lett.* 257, 391–406.
- Sarda, P., Moreira, M., Staudacher, T., Schilling, J.-G., Allègre, C.J., 2000. Rare gas systematics on the southernmost Mid-Atlantic Ridge: constraints on the lower mantle and the Dupal source. *J. Geophys. Res., Solid Earth* 105, 5973–5996.
- Schilling, J.-G., 1991. Fluxes and excess temperatures of mantle plumes inferred from their interaction with migrating mid-ocean ridges. *Nature* 352, 397–403.
- Schilling, J.G., Fontignie, D., Blichert-Toft, J., Kingsley, R., Tomza, U., 2003. Pb–Hf–Nd–Sr isotope variations along the Galápagos Spreading Center (101°–83°W): constraints on the dispersal of the Galápagos mantle plume. *Geochem. Geophys. Geosyst.* 4. <https://doi.org/10.1029/2002GC000495>.
- Shimizu, K., Saal, A.E., Myers, C.E., Nagle, A.N., Hauri, E.H., Forsyth, D.W., Kamenetsky, V.S., Niu, Y., 2016. Two-component mantle melting-mixing model for the generation of mid-ocean ridge basalts: implications for the volatile content of the Pacific upper mantle. *Geochim. Cosmochim. Acta* 176, 44–80.
- Simons, K., Dixon, J., Schilling, J.-G., Kingsley, R., Poreda, R., 2002. Volatiles in basaltic glasses from the Easter–Salas y Gómez Seamount Chain and Easter Microplate: implications for geochemical cycling of volatile elements. *Geochem. Geophys. Geosyst.* 3, 1–29.
- Sinton, J.M., 2003. Morphology and segmentation of the western Galápagos Spreading Center, 90.5°–98°W: plume–ridge interaction at an intermediate spreading ridge. *Geochem. Geophys. Geosyst.* 4. <https://doi.org/10.1029/2003GC000609>.
- Sleep, N., 2008. Channeling at the base of the lithosphere during the lateral flow of plume material beneath flow line hot spots. *Geochem. Geophys. Geosyst.* 9. <https://doi.org/10.1029/2008GC002090>.
- Stroncik, N.A., Devey, C.W., 2011. Recycled gabbro signature in hotspot magmas unveiled by plume–ridge interactions. *Nat. Geosci.* 4, 393–397.
- Stroncik, N.A., Niedermann, S., Haase, K.M., 2008. Plume–ridge interaction revisited: evidence for melt mixing from He, Ne and Ar isotope and abundance systematics. *Earth Planet. Sci. Lett.* 268, 424–432.